Evidence from first-principles calculations for orbital ordering in Ba_2NaOsO_6: A Mott insulator with strong spin-orbit coupling

R. Cong,[1] Ravindra Nanguneri,[2] Brenda Rubenstein,[2,*] and V. F. Mitrović[1,†]
[1]*Department of Physics, Brown University, Providence, Rhode Island 02912, USA*
[2]*Department of Chemistry, Brown University, Providence, Rhode Island 02912, USA*

(Received 17 June 2019; revised manuscript received 21 October 2019; published 24 December 2019)

We present first-principles calculations of the magnetic and orbital properties of Ba_2NaOsO_6 (BNOO), a $5d^1$ Mott insulator with strong spin-orbit coupling (SOC) in its low-temperature emergent quantum phases. Our computational method takes into direct consideration recent NMR results that established that BNOO develops a local octahedral distortion preceding the formation of long-range magnetic order. We found that the two-sublattice canted ferromagnetic ground state identified in Lu *et al.*, [Nat. Commun. **8**, 14407 (2017)] is accompanied by a two-sublattice staggered orbital ordering pattern in which the t_{2g} orbitals are selectively occupied as a result of strong spin-orbit coupling. The staggered orbital order found here using first-principles calculations asserts the previous proposal of Chen *et al.*, [Phys. Rev. B **82**, 174440 (2010).] and Lu *et al.*, [Nat. Commun. **8**, 14407 (2017).] that a two-sublattice magnetic structure is the very manifestation of staggered quadrupolar order. Therefore, our results affirm the essential role of multipolar spin interactions in the microscopic description of magnetism in systems with locally entangled spin and orbital degrees of freedom.

DOI: 10.1103/PhysRevB.100.245141

I. INTRODUCTION

The competition between electron correlation and spin-orbit coupling (SOC) present in materials containing 4- and 5*d* transition metals is an especially fruitful tension predicted to lead to the emergence of a plethora of exotic quantum phases, including quantum spin liquids, Weyl semimetals, Axion insulators, and phases with exotic magnetic orders [1–11]. There has been an active quest to develop microscopic theoretical models to describe such systems with comparably strong correlations and SOC to enable the prediction of their emergent quantum properties [1–5]. In strong Mott insulators, mean-field theories predict strong SOC to partially lift the degeneracy of total-angular-momentum eigenstates by entangling orbital and spin degrees of freedom to produce highly nontrivial anisotropic exchange interactions [2,3,5,7]. These unusual interactions are anticipated to promote quantum fluctuations that generate such novel quantum phases as an unconventional antiferromagnet with dominant magnetic octupole and quadrupole moments and a noncollinear ferromagnet whose magnetization points along the [110] axis and possesses a two-sublattice structure.

Because their SOC and electron correlations are of comparable magnitude [6], 5*d* double perovskites ($A_2BB'O_6$) are ideal materials for testing these predictions. Indeed, recent NMR measurements on a representative material of this class, Ba_2NaOsO_6 (BNOO), revealed that it possesses a form of exotic ferromagnetic order: A two-sublattice canted ferromagnetic (cFM) state, reminiscent of theoretical predictions [12]. Specifically, upon lowering its temperature, BNOO evolves from a paramagnetic (PM) state with perfect fcc cubic symmetry into a broken local point symmetry (BLPS) state. This BLPS phase precedes the formation of long-range magnetic order, which at sufficiently low temperatures coexists with the two-sublattice cFM order, with a net magnetic moment of $\approx 0.2\,\mu_B$ per osmium atom along the [110] direction. One key question that remains is whether such cFM order implies the existence of complex orbital/quadrupolar order.

In this paper, we report a two-sublattice orbital ordering pattern that coexists with cFM order in BNOO, as revealed by DFT+U calculations. Evidence for this order is apparent in BNOO's selective occupancy of the t_{2g} orbitals and spin-density distribution. More specifically, the staggered orbital pattern is manifest in BNOO's partial density of states and band structure, which possesses a distinct t_{2g} orbital contribution along high-symmetry lines. This staggered orbital pattern is not found in the FM[110] phase. The results of our first-principles calculations paint a coherent picture of the coexistence of cFM order with staggered orbital ordering in the ground state of BNOO. Therefore, the staggered orbital order discovered here validates the previous proposal that the two-sublattice magnetic structure, which defines the cFM order in BNOO, is the very manifestation of staggered quadrupolar order with distinct orbital polarization on the two sublattices [2,12]. Furthermore, our results affirm that multipolar spin interactions are an essential ingredient of quantum theories of magnetism in SOC materials.

This paper is organized as follows. The details of our first-principles density functional theory (DFT) calculations of NMR observables is first described in Sec. II. In Sec. III, we present our numerical results for the nature of the orbital order for a given imposed magnetic state. Lastly, in Sec. IV,

*Corresponding author: vemi@brown.edu
†Corresponding author: brenda_rubenstein@brown.edu

we conclude with a summary of our current findings and their bearing on the physics of related materials.

II. COMPUTATIONAL APPROACH

All of the following computations were performed using the Vienna Ab initio Simulation Package (VASP), complex version 5.4.1/.4, plane-wave basis DFT code [13–16] with the generalized gradient approximation (GGA) PW91 [17] functional and two-component spin-orbit coupling. We used 500 eV as the plane-wave basis cutoff energy, and we sampled the Brillouin zone using a $10 \times 10 \times 5$ k-point grid. The criterion for stopping the DFT self-consistency cycle was a 10^{-5}-eV difference between successive total energies. Two tunable parameters, U and J, were employed. U describes the screened-Coulomb density-density interaction acting on the Os $5d$ orbitals, and J is the Hund's interaction that favors maximizing S^z_{total} [18]. In this work, we set $U = 3.3$ eV and $J = 0.5$ eV based upon measurements from Ref. [12] and calculations in Ref. [21]. We note that these parameters are similar in magnitude to those of the SOC contributions we observe in the simulations presented below, which are between 1 and 2 eV. This is in line with previous assertions that the SOC and Coulomb interactions in $5d$ perovskites are similar in magnitude. Projector augmented wave (PAW) [19,20] pseudopotentials (PPs) that include the p semicore orbitals of the Os atom, which are essential for obtaining the observed electric field gradient (EFG) parameters [21], were employed to increase the computational efficiency. A monoclinic unit cell with P2 symmetry is required to realize cFM order [see Supplemental Material [22] for the detailed description of the considered unit cell [23] (and Ref. [2] therein)]. The lattice structure with BLPS characterized by the orthorhombic Q2 distortion mode that was identified as being in the best agreement with NMR findings and referred to as Model A.3 in Ref. [21] was imposed.

The general outline of the calculations we performed is described in the following. We first carried out single self-consistent or "static" calculations with GGA+SOC+U with a fixed BLPS structure for model A, representing the orthorhombic Q2 distortion mode. Then, a magnetic order with [110] easy axes, as dictated by experimental findings [12,24], is imposed on the osmium lattices. Typically, we found that the final moments converged to nearly the same directions as the initial ones. Specifically, two types of such initial order are considered: (a) simple FM order with spins pointing along the [110] direction; and (b) noncollinear, cFM order in which initial magnetic moments are imposed on the two osmium sublattices in the directions determined in Ref. [12]. We used the Methfessel-Paxton (MP) smearing technique [25] to facilitate charge-density convergence. For the density of states and band structure calculations, we employed the tetrahedron smearing with Blöchl corrections [26] and Gaussian methods, respectively.

III. ORBITAL ORDERING WITH IMPOSED MAGNETIC CFM AND FM110 ORDERS

In the following sections, we report our results for the orbital order, band structure, and density of states of BNOO when we impose magnetic order with [110] easy axes and the local orthorhombic distortion that best matched experiments [21]. In Table I, we summarize the converged orbital and spin magnetic moments. In BNOO, $M = 2S + L_{\text{eff}} = 0$, since the t_{2g} level can be regarded as a pseudospin with $L_{\text{eff}} = -1$. The magnitude of the spin moment, $|\vec{S}|$, is in the vicinity of $\approx 0.5\mu_B$, while the orbital moment, $|\vec{L}|$, is $\approx 0.4\mu_B$. These values are reduced from their purely local moment limit due to hybridization with neighboring atoms, and, in the case of $\vec{L}$, by quenching caused by the distorted crystal field. For imposed cFM order, we find that the relative angle ϕ between the two sublattices is in agreement with our NMR findings in Ref. [12]. Indeed, first-principles calculations, performed outside of our group, taking into account multipolar spin interactions found that the reported canted angle of $\approx 67^\circ$ corresponds to the global energy minimum [27].

TABLE I. cFM and FM[110] magnetic moments for the imposed representative BLPS structure using GGA+SOC+U. The angles, ϕ, are in degrees and measured anticlockwise with respect to the $+x$ axis. The magnitudes of spin, orbital, and total moments are denoted by $|\vec{S}|$, $|\vec{L}|$, and $|\vec{M}|$, in units of μ_B, respectively. The small net magnetic moment is due to the antialignment of $\vec{S}$ and $\vec{L}_{\text{eff}}$ in the $J_{\text{eff}} = \frac{3}{2}$ state. As of now, the FM110 state has not been experimentally identified in a $5d$ double perovskite.

	$\lvert\vec{S}\rvert$	$\phi(S)$	$\lvert\vec{L}\rvert$	$\phi(L)$	M	$\phi(M)$
cFM						
Os1	0.55	–41.56	0.44	$90 + 46.29$	0.12	–34
Os2	0.55	$90 + 28.73$	0.43	-31.07	0.11	110
FM110						
Os	0.83	45	0.52	225	0.31	45

Next, we will explore the nature of the orbital ordering. Previous first-principles works hinted at the presence of orbital order in BNOO but did not fully elucidate its nature [28]. Since we imposed cFM order and SOC, we were able to obtain a more exotic orbital order than uniform ferro order. We report below evidence for a type of layered, anti-ferro-orbital-order (AFOO) that has been shown to arise in the mean-field treatment of multipolar Heisenberg models with SOC [5].

First, we analyze the nature of the orbital order by computing the spin density. The spin density is a continuous vector field of the electronic spin and can point in noncollinear directions. Its operators are the product of the electrons' density and their spin-projection operators, such as $\Delta^z(\vec{r}) = \sum_i \delta(\vec{r}_i - \vec{r}) S^z_i$.

The spin densities are given by the expectation value

$$\langle \Delta^z(\vec{r}) \rangle = Tr[\rho_d \Delta^z(\vec{r})], \tag{1}$$

where ρ_d is the $5d$-shell single-particle density matrix obtained from DFT+U calculations. In Fig. 1, the $\langle \Delta^{x,y,z}(\vec{r}) \rangle$, obtained via GGA+SOC+U calculations, are displayed for two distinct Os sublattices. The results illustrate that the spins are indeed localized about the Os atoms and that there is a noticeable imbalance in the distribution of the $n_\uparrow$ and $n_\downarrow$ spin densities, which manifests in their difference, $\langle \Delta^z(\vec{r}) \rangle \equiv n_\uparrow(\vec{r}) - n_\downarrow(\vec{r})$. The difference in the spatial distribution between the two sublattice spin densities is indicative of the orbital ordering. The net spin moments are obtained by

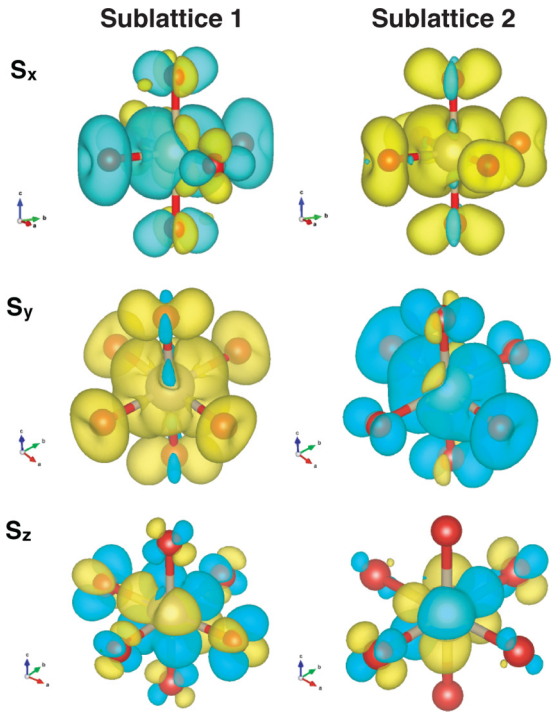

FIG. 1. Contour plots of the spin density on two distinct sublattices of the BLPS structure (model A.3 in Ref. [21]) from GGA+SOC+U calculations. The S_x (top row), S_y (center row), and S_z (bottom row) components of the spin density on a single Os octahedron from sublattice 1 (left column) and sublattice 2 (right column) are plotted. The different colors denote the signs of the $S_{x,y,z}$ projections. The isovalues are blue for positive $S_{x,y,z}$, 0.001 and yellow for negative $S_{x,y,z}$, −0.001. On the top left, the negative S_x density is sandwiched between the lobes of the positive S_x densities on the Os atom, and vice versa for the Os atom on the top right. On the top left, four of the O atoms have a cloverleaf spin-density pattern with alternating positive and negative S_x densities, while on the top right, only the two axial O atoms have this pattern. The other O atoms in the top two OsO_6 octahedra have spin densities that are uniformly polarized.

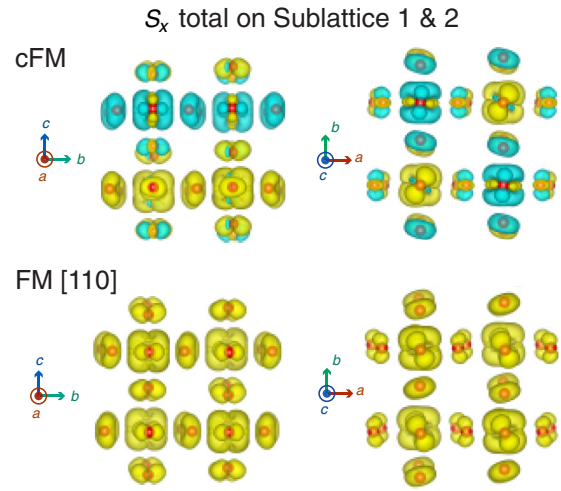

FIG. 2. Two views of the S_x component of the spin density for imposed FM order and an orthorhombic Q2 distortion (model A.3 in Ref. [21] on both sublattices as viewed along the a and c directions. This component shows only the S_x projection of the spin vector field. The isovalues are blue, positive S_x: 0.001, and yellow, negative S_x: −0.001.

integrating the spin density over the volume of a sphere enclosing the Os atoms.

In Fig. 1, the following is visually clear: (i) the S^x (top) and S^y (center) spin-density components are overwhelmingly of a single sign, which gives rise to net moments in the (a, b) plane; and (ii) the signs of S^x and S^y between the two sublattices are reversed, indicating that the sublattice spins are canted symmetrically about the [110] direction and the angle between them exceeds 90°. In contrast, for S^z (bottom), both signs of S^z contribute equally so that the net $S^z \approx 0$ after integrating over the sphere.

In Fig. 2, we plot the total S_x component of the spin density over two sublattices for both types of imposed magnetic order. It is evident that the staggered orbital pattern only arises when cFM order is imposed. Therefore, we demonstrate that the staggered orbital order can solely coexist with cFM order.

We note also that in Figs. 1 and 2 there is non-negligible spin density on the O atoms of the OsO_6 octahedra. It is usually thought that atoms with closed shells, like O in stoichiometric compounds, possess negligible spin densities. This is an unexpected feature in BNOO that has been previously noted in Ref. [28] and is due to the stronger $5d$-$2p$ hybridization, which results in OsO_6 cluster orbitals. The spin imbalance is a quantity associated with the cluster rather than the individual atoms, which is why we see the spin densities on the O atoms.

For noncollinear systems, the orbital character of each osmium's $5d$ manifold can be further decomposed into the Cartesian components of the spin magnetization: $\langle S_i \rangle \equiv M_i$, $i = x, y, z$. Since the spins lie in the (xy) plane and the M_z component is zero for both sublattices, we plotted only M_x, M_y, and the total partial density of states (PDOS) for the two sublattices. We see in Fig. 3 that, first, for both sublattices, only the t_{2g} orbitals have an appreciable density of states, consistent with the fact that the calculated d occupation at the Os sites is $\langle n_d \rangle < 6$. Second, below the band gap, the d_{yz} orbital has the same occupation on both sublattices, while the d_{xy} orbital is occupied on one sublattice and the d_{zx} orbital on the other. This pattern in which certain d orbitals are preferentially occupied at different sites deviates from the case without orbital ordering, in which each of the d_{xy}, d_{yz}, and d_{zx} orbitals have the same occupancies on both Os sites, as shown in Ref. [27]. These orbital occupations are consistent with mean-field predictions of the occupancy of the Os d orbitals at zero temperature, which also predict a staggered pattern [5]. This staggered pattern arises from BNOO's distinctive blend of cFM order with strong SOC.

To study this ordering in greater depth, we can compute the occupation matrices, which after diagonalization, yield the occupation number (ON) eigenvalues and corresponding natural orbital (NO) eigenvectors. For a given Os atom, the $5d$ spin orbitals have unequal amplitudes in each NO, as expected for the AFOO. The NOs also all have different occupation numbers. Regardless of their precise occupations, the unequal spin-orbital superpositions in the NOs endow the Os with

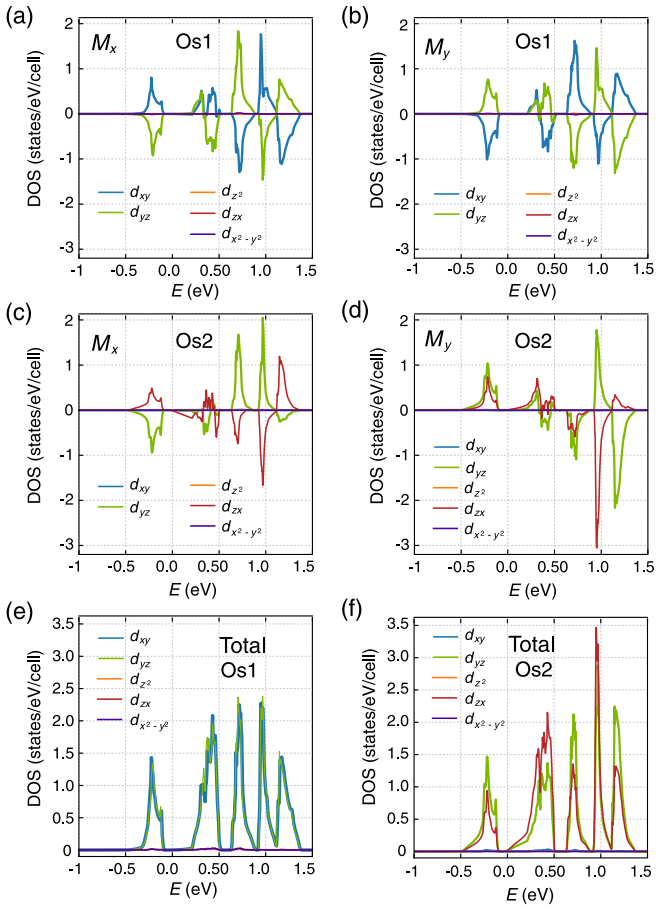

FIG. 3. The partial density of states (PDOS) for spin decomposed parts of the Q2 orthorhombic distortion (model A.3 in Ref. [21]) for the Os atom in each sublattice, Os1 and Os2.

a net nonzero spin and orbital moment. We moreover note that, due to $5d$-$2p$ hybridization, there is significant charge transfer from O to Os, such that the charge on the $5d$ shell of osmium is $\langle n_d \rangle \approx 5$–$6$, which is very different from the nominal heptavalent $5d^1$ filling from simple valence counting. Furthermore, the ten NOs are fractionally occupied with the largest ON close to $\langle n_1 \rangle \approx 1.0$ and the other nine NOs having occupations ranging from 0.37 to 0.56. For the NO, $|1\rangle$, with the occupation $\langle n_1 \rangle \approx 1.0$, the coefficients of the e_g orbitals are an order of magnitude smaller than those for the t_{2g} orbitals.

In Fig. 4, we plot the band structures of the two sublattice Os atoms along the high-symmetry directions of the monoclinic cell, with the total partial characters of the Os $5d$ bands color-coded proportional to their squared-amplitude contributions to the Kohn-Sham eigenvectors, the so-called fat bands. The total partial character is the root of the sum of the squares of the partial characters of the Cartesian spin projections, $\sqrt{M_x^2 + M_y^2 + M_z^2}$. We plot the partial characters of the spin projections of M_x and M_y in the Supplemental Material Figs. 3 and 4 [22], but not M_z because it is two orders of magnitude smaller than the other two. For both Os atoms along these high-symmetry directions, only t_{2g} orbitals are occupied, consistent with $\langle n_d \rangle < 6$. The t_{2g} and e_g are irreducible representations of perfect cubic, octahedral, or tetrahedral symmetry. Because these symmetries are broken in the structure with Q2 distortion, there are no pure t_{2g} or e_g orbitals, nor a $\Delta(e_g - t_{2g})$ energy splitting, and there will be a small mixing between the two sets of orbitals.

We see that for both sublattices, below the band gap, the d_{yz} orbital is most heavily occupied (as denoted by the brighter green color), especially along the X_1-M_2 direction, while the d_{xy} and d_{zx} orbitals are less occupied. However, around the Γ

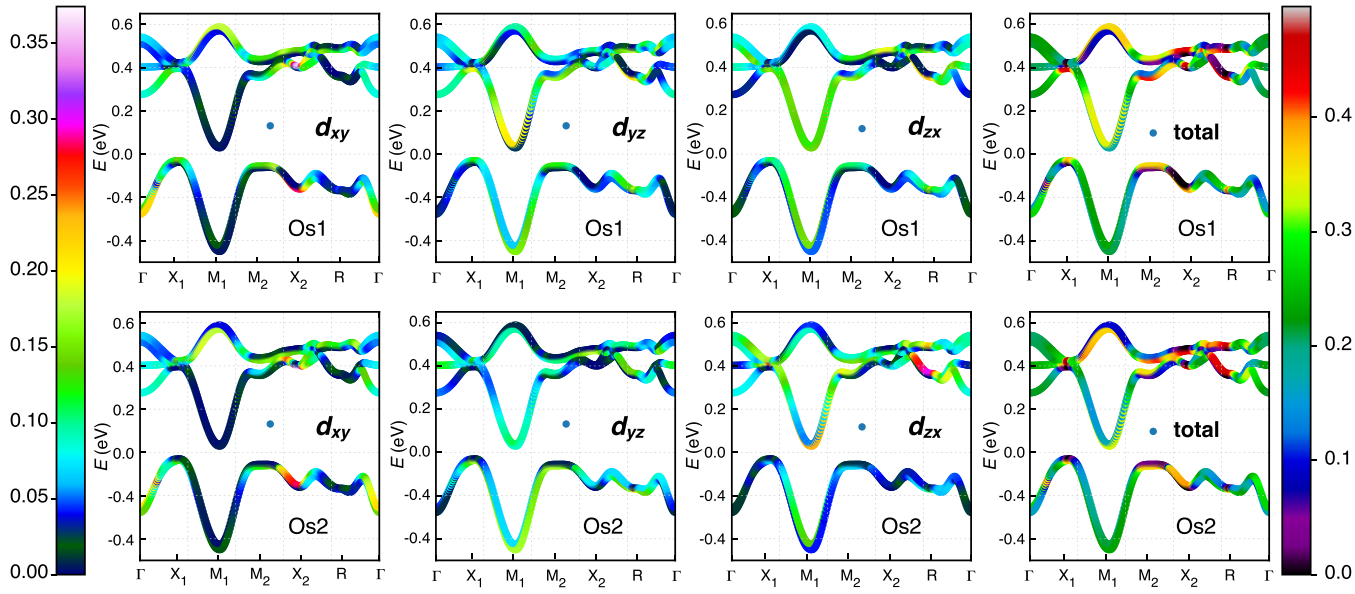

FIG. 4. The band structures of the two sublattice Os atoms near the Fermi level with $5d$ partial characters for the Q2 orthorhombic distortion (model A.3 in Ref. [21]): Os1 sublattice (top), Os2 sublattice (bottom). The projection of each $5d$ orbital onto the Kohn-Sham bands is represented by the color shading. The color bar on the left shows the color scaling for the partial characters of the t_{2g} orbitals, while the color bar on the right shows the scaling for all of the orbitals. The chosen high-symmetry points are $\Gamma = (0,0,0)$, $X_1 = (\frac{1}{2},0,0)$, $M_1 = (0,\frac{1}{2},0)$, $M_2 = (\frac{1}{2},0,\frac{1}{2})$, $X_2 = (0,0,\frac{1}{2})$, and $R = (0, \frac{1}{2},\frac{1}{2})$.

point, the d_{xy} orbital obviously has the largest occupancy. We point out that here the d orbital character contribution is only for the selected high-symmetry directions. Thus, it cannot be directly compared with the PDOS result. Nevertheless, the different orbital character contributions reflected in the color can also be observed for all three t_{2g} orbitals, especially along the X_2-Γ line. We can also see that the dispersions are largest along the X_1-M_2 and X_1-Γ paths, while the bands are flatter from M_2 to R. The band gap is indirect and $\approx$0.06 eV in magnitude.

Finally, we have computed the gaps for the imposed cFM phase. We found that the gaps for the cFM phase with the DFT+U parameters of $U = 3.3$ eV and $J = 0.5$ eV are finite but too small to be considered Mott insulating gaps. However, we find that the gap opens dramatically as we raise U to 5.0 eV, as shown in detail in the Supplemental Material [22]. In fact, even a "small" increase to $U = 4.0$ eV is sufficient to open the gap to $E_{\text{gap}} = 0.244$ eV. This indicates that the true value of U for the osmium $5d$ shell in BNOO could plausibly approach 4.0 eV but not exceed it. Previously, it was found that LDA+U with $U = 4$ eV $> W$ was insufficient to open a gap [29–31]. Here, we demonstrated that GGA+SOC+U is sufficient to open a gap for $U \approx 4.0$ eV.

IV. CONCLUSIONS

In this work, we carried out DFT+U calculations on the magnetic Mott insulator Ba_2NaOsO_6, which has strong spin-orbit coupling. Our numerical work is inspired by our recent NMR results revealing that this material exhibited a broken local point symmetry (BLPS) phase followed by a two-sublattice exotic canted ferromagnetic order (cFM). The local symmetry is broken by the orthorhombic Q2 distortion mode [21]. The question we addressed here is whether this distortion is accompanied by the emergence of orbital order. It was previously proposed that the two-sublattice magnetic structure, revealed by NMR, is the very manifestation of staggered quadrupolar order with distinct orbital polarization on the two sublattices arising from multipolar exchange interactions [2,12]. Moreover, it was indicated via a different mean-field formalism that the anisotropic interactions result in orbital order that stabilizes exotic magnetic order [5]. Therefore, distinct mean-field approaches [2,5] with a common ingredient of anisotropic exchange interactions imply that exotic magnetic order, such as the cFM reported in Ref. [12], is accompanied/driven by an orbital order.

Motivated by the cFM order detected in NMR experiments, here we investigated BNOO's orbital ordering pattern from first principles. We found two-sublattice orbital ordering, illustrated by the spin-density plots, within the alternating planes in which the total magnetic moment resides. An auxiliary signature of the orbital ordering is revealed by the occupancies of the t_{2g} orbitals in the density of states and band structures. Our first-principles work demonstrates that this two-sublattice orbital ordering mainly arises from cFM order and strong SOC. Moving forward, it would be worthwhile to more thoroughly investigate the cFM order observed in this work using other functionals or methods more adept at handling strong correlation to eliminate any ambiguities that stem from our specific computational treatment.

ACKNOWLEDGMENTS

The authors thank J.-P. Song and Y. Zhang for enlightening discussions. We are especially grateful to Ian Fisher for his long-term collaboration on the physics of Ba_2NaOsO_6. This work was supported in part by US National Science Foundation through Grants No. DMR-1608760 (V.F.M.) and No. DMR-1726213 (B.M.R.). The calculations presented here were performed using resources at the Center for Computation and Visualization, Brown University.

[1] B. J. Kim, H. Jin, S. J. Moon, J.-Y. Kim, B.-G. Park, C. S. Leem, J. Yu, T. W. Noh, C. Kim, S.-J. Oh, J.-H. Park, V. Durairaj, G. Cao, and E. Rotenberg, Phys. Rev. Lett. **101**, 076402 (2008).
[2] G. Chen, R. Pereira, and L. Balents, Phys. Rev. B **82**, 174440 (2010).
[3] G. Chen and L. Balents, Phys. Rev. B **84**, 094420 (2011).
[4] H. Ishizuka and L. Balents, Phys. Rev. B **90**, 184422 (2014).
[5] C. Svoboda, M. Randeria, and N. Trivedi, arXiv:1702.03199v1.
[6] W. Witczak-Krempa, G. Chen, Y. B. Kim, and L. Balents, Ann. Rev. Condens. Matter Phys. **5**, 57 (2014).
[7] J. Romhányi, L. Balents, and G. Jackeli, Phys. Rev. Lett. **118**, 217202 (2017).
[8] B. J. Kim, H. Ohsumi, T. Komesu, S. Sakai, T. Morita, H. Takagi, and T. Arima, Science **323**, 1329 (2009).
[9] H. Zhang, K. Haule, and D. Vanderbilt, Phys. Rev. Lett. **111**, 246402 (2013).
[10] S. J. Moon, H. Jin, K. W. Kim, W. S. Choi, Y. S. Lee, J. Yu, G. Cao, A. Sumi, H. Funakubo, C. Bernhard, and T. W. Noh, Phys. Rev. Lett. **101**, 226402 (2008).
[11] X. Wan, A. M. Turner, A. Vishwanath, and S. Y. Savrasov, Phys. Rev. B **83**, 205101 (2011).
[12] L. Lu, M. Song, W. Liu, A. P. Reyes, P. Kuhns, H. O. Lee, I. R. Fisher, and V. F. Mitrović, Nat. Commun. **8**, 14407 (2017).
[13] G. Kresse and J. Hafner, Phys. Rev. B **47**, 558 (1993).
[14] G. Kresse and J. Hafner, Phys. Rev. B **49**, 14251 (1994).
[15] G. Kresse and J. Furthmuller, Comput. Mater. Sci. **6**, 15 (1996).
[16] G. Kresse and J. Furthmuller, Phys. Rev. B **54**, 11169 (1996).
[17] J. P. Perdew and Y. Wang, Phys. Rev. B **45**, 13244 (1992).
[18] F. Z. Hund, Z. Phys. **33**, 345 (1925).
[19] P. E. Blöchl, Phys. Rev. B **50**, 17953 (1994).
[20] G. Kresse and D. Joubert, Phys. Rev. B **59**, 1758 (1999).
[21] R. Cong, R. Nanguneri, B. M. Rubenstein, and V. F. Mitrovic, arXiv:1908.09014.
[22] See Supplemental Material at http://link.aps.org/supplemental/10.1103/PhysRevB.100.245141 for a detailed description of the considered unit cell, plots of the partial characters of the spin projections of M_x and M_y (Figs. 3 and 4) (the M_z projection is not shown because it is 2 orders of magnitude smaller than the other two), and details of the gap evolution as a function of U.

[23] K. E. Stitzer, M. D. Smith, and H.-C. zur Loye, Solid State Sciences **4**, 311 (2002).
[24] A. S. Erickson, S. Misra, G. J. Miller, R. R. Gupta, Z. Schlesinger, W. A. Harrison, J. M. Kim, and I. R. Fisher, Phys. Rev. Lett. **99**, 016404 (2007).
[25] M. Methfessel and A. T. Paxton, Phys. Rev. B **40**, 3616 (1989).
[26] P. E. Blöchl, O. Jepsen, and O. K. Andersen, Phys. Rev. B **49**, 16223 (1994).
[27] D. F. Mosca, Master's thesis, Università di Bologna, 2019.
[28] S. Gangopadhyay and W. E. Pickett, Phys. Rev. B **91**, 045133 (2015).
[29] K.-W. Lee and W. E. Pickett, Europhys. Lett. **80**, 37008 (2007).
[30] H. J. Xiang and M.-H. Whangbo, Phys. Rev. B **75**, 052407 (2007).
[31] S. Gangopadhyay and W. E. Pickett, Phys. Rev. B **93**, 155126 (2016).